Toward Lossless Infrared Optical Trapping of Small Nanoparticles Using Nonradiative Anapole Modes

J. J. Hernández-Sarria,[1] Osvaldo N. Oliveira, Jr.[1] and J. R. Mejía-Salazar[2,*]

[1]*Instituto de Física de São Carlos, Universidade de São Paulo, CP 369, 13560-970, São Carlos, SP, Brasil*
[2]*Instituto Nacional de Telecomunicações (Inatel), 37540-000, Santa Rita do Sapucaí, MG, Brazil*

A challenge in plasmonic trapping of small nanoparticles is the heating due to the Joule effect of metallic components. This heating can be avoided with electromagnetic field confinement in high-refractive-index materials, but nanoparticle trapping is difficult because the electromagnetic fields are mostly confined inside the dielectric nanostructures. Herein, we present the design of an all-dielectric platform to capture small dielectric nanoparticles without heating the nanostructure. It consists of a Si nanodisk engineered to exhibit the second-order anapole mode at the infrared regime ($\lambda = 980$ nm), where Si has negligible losses, with a slot at the center. A strong electromagnetic hot spot is created, thus allowing us to capture nanoparticles as small as 20 nm. The numerical calculations indicate that optical trapping in these all-dielectric nanostructures occurs without heating only in the infrared, since for visible wavelengths the heating levels are similar to those in plasmonic nanostructures.

Optical tweezers with particle trapping by optical fields [1–3] have been used to manipulate micron-sized particles [4–10], DNA molecules [11], low-dimensional semiconductor structures [12], and metallic [13] nanoparticles [14]. These tools are limited when dealing with minute nanoparticles, i.e., much smaller than the incident wavelength (λ). Since the trapping force follows an r^3 law [2], where r is the radius of a spherical nanoparticle, there is an abrupt drop with decreasing r. The trapping well becomes shallower while its minimum depth should be $-10 k_B T$ (k_B is the Boltzmann constant and T is the absolute temperature in the trap) to avoid nanoparticle diffusing out of the trap by Brownian motion [2]. Therefore, a stable optical trapping of small nanoparticles requires high-power, tightly focused laser beams, which may be unavailable or photodamage temperature-sensitive particles. Moreover, conventional optical tweezers use beams that can only be focused to a diffraction-limited spot, and trapping is thus loose with potentials distributed over regions much larger than the trapped nanoparticles. These issues have been addressed with strongly enhanced and localized plasmonic fields (plasmonic hot spots), the leading approach for small nanoparticle trapping [15–21]. Nevertheless, Joule heating of metallic plasmonic platforms hampers applications with biologically relevant molecules [22], as the losses associated with plasmonic resonances may result in boiling water even for incident optical intensities of only 8 mW/μm^2 [20].

An alternative for low-loss electromagnetic field confinement and enhancement consists in exploiting the electromagnetic resonances of high-refractive-index dielectric nanostructures [23]. The excitation of nonradiating anapole modes leads to concentrated electromagnetic energy inside a single dielectric nanodisk or in an arrangement of nanodisks [24–27]. An anapole mode arises from a composition of electrical and toroidal dipole moments with destructive interference of the corresponding far-field radiation patterns and leads to energy concentration inside the particle. This effect is exploited for third harmonic generation [25] through excitation of second-order anapole states within the near-infrared wavelength range. These higher-order anapole states exhibit sharper resonances with stronger energy concentration, as observed for Si nanodisks on silica wafers [26]. However, the electromagnetic field inside elementary scatterers should be inaccessible for interaction with nearby molecules or particles, a limitation surpassed recently [28,29]. In particular, small slots in dielectric nanodisks yielded subwavelength external hot spots with electric field enhancements of up to 3 orders of magnitude [28,29], thus being accessible to nearby molecules.

In this Letter, we propose all-dielectric nanostructures for lossless optical trapping of small nanoparticles based on the electromagnetic field confinement associated with the second-order anapole mode of a single-slotted dielectric nanodisk. The nanodisk was designed to exhibit the anapole mode at the infrared where there is efficient optical trapping of subwavelength dielectric nanoparticles with diameters as small as $D = 20$ nm. We considered a Gaussian laser beam with incident power of 100 mW and numerical aperture 0.85 impinging from the substrate, i.e., with smaller intensity than in optical tweezers with propagating beams. We demonstrate heating of resonant dielectric nanostructures due to displacement currents for

visible and near-infrared wavelengths. As in experimental work [24], we considered the nanodisk made of amorphous silicon, a glass substrate and water in the surrounding medium. The induced optical force on the nanoparticles is calculated through a rigorous treatment with the conservation law for momentum [6,30]

$$\mathbf{F} = \frac{d}{dt}(\mathbf{P}_{\mathrm{mec}} + \mathbf{P}_{\mathrm{em}}) = \oint_S \overset{\leftrightarrow}{T} \cdot d\mathbf{S}, \qquad (1)$$

where $\mathbf{P}_{\mathrm{mec}}$ and $\mathbf{P}_{\mathrm{em}} = (\varepsilon\mu/c^2) \int_V \mathbf{S}\, dV$ are the mechanical momentum and the electromagnetic field momentum, respectively, inside a surface S enclosing the nanoparticle. ε and μ represent the permittivity and permeability of the medium, respectively. $\overset{\leftrightarrow}{T}$ is used for the Maxwell's stress tensor, given by [6,30]

$$\overset{\leftrightarrow}{T} = \varepsilon\mathbf{E}\mathbf{E} + \mu\mathbf{H}\mathbf{H} - \frac{1}{2}(\varepsilon E^2 + \mu H^2)\overset{\leftrightarrow}{I}, \qquad (2)$$

where $\mathbf{E}\mathbf{E}$ ($\mathbf{H}\mathbf{H}$) denotes the outer product and $\overset{\leftrightarrow}{I}$ represents the unit dyad [31]. Calculating the time average the field momentum contribution goes to zero and the mechanical average force becomes [6]

$$\langle\mathbf{F}\rangle = \oint_S \langle\overset{\leftrightarrow}{T}\rangle \cdot d\mathbf{S}, \qquad (3)$$

where the integration is performed for the nanoparticle within a closed surface. The finite difference time-domain (FDTD) method was used within FDTD Solutions (Lumerical Inc., Canada) to solve the electromagnetic fields, forces and effective potentials. The force field map and effective potential were obtained by repeating the calculations at different center positions ($\mathbf{r}_0$). Since the force is calculated for conservative systems, for wavelengths where the imaginary permittivity component [Im(ε)] is zero for the nanoparticle and surrounding medium, an effective transverse potential is [32]

$$U(\mathbf{r}_0) = -\int_\infty^{\mathbf{r}_0} \langle\mathbf{F}_{xy}(\mathbf{r})\rangle \cdot d\mathbf{r}. \qquad (4)$$

The working principle is illustrated with Fig. 1 where a nanodisk of amorphous silicon with radius $R = 420$ nm and height $h = 100$ nm is placed on a semi-infinite glass substrate. The system is surrounded by water and the incident linearly polarized Gaussian beam impinges from below. The electric field component of light is parallel to the y axis. The length and width of the slotted region are selected to produce high electromagnetic field enhancements, since geometry affects the poloidal currents [29]. We used $l = \frac{2}{3}R = 280$ nm for the slot length to optimize field enhancement inside the slot at the second-order anapole mode [29]. The width was $w = 25$ nm for field
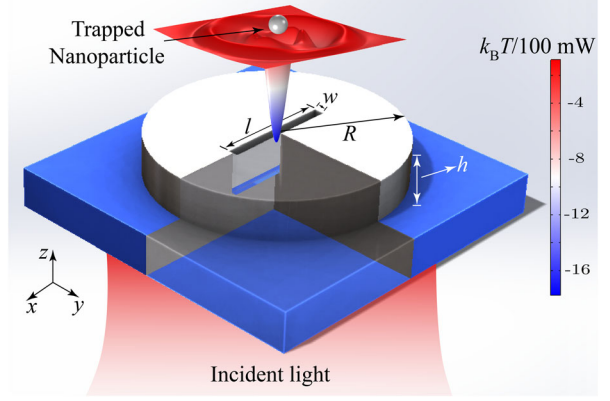

FIG. 1. Optical effective transverse potential and schematic representation of the high-refractive-index resonant nanostructure. The nanodisk is illuminated with a linearly polarized Gaussian laser beam from the bottom. The nanoparticle with $r = 15$ nm and $n_{\mathrm{np}} = 2.0$ is placed 20 nm above the nanodisk, which is trapped by the near-field transmitted through the structure. The substrate is considered semi-infinite.

enhancement. The effective potential for a dielectric spherical nanoparticle with radius $r = 15$ nm and refractive index $n_{\mathrm{np}} = 2.0$ is shown above the structure representation in Fig. 1. Results were calculated under resonant condition, i.e., for $\lambda = 980$ nm, as discussed below. The nanoparticle placed 20 nm above the nanodisk is also illustrated. The nanoparticle refractive index was set to an intermediate value between proteins ($n \approx 1.6$) and semiconductor quantum dots ($n \approx 2.4$) [33,34] to emphasize the suitability to manipulate those kinds of nanoparticles. As observed from the color scale, a stable transverse optical trapping ($U < -10k_BT$) is expected for this nanoparticle.

The design of the resonant dielectric nanostructure was inspired by the strong electromagnetic field enhancement in the slot region of a single-slotted silicon nanodisk in air, where energy concentration was stronger with narrower resonances for the second-order anapole mode than with the first order mode [29]. This facilitates applying the concept in realistic scenarios with the silicon nanodisk on a glass substrate surrounded by water. Stable optical trapping of small nanoparticles is made possible, as shown in Fig. 1. The anapole modes are defined as the scattering dark states due to the superposition of electric and toroidal dipole moments, resulting in suppression of energy radiation. In high-refractive-index dielectric nanodisks these modes can be reached through high diameter-to-thickness aspect ratios [24]. As we seek resonances above $\lambda = 950$ nm, where Im(ε) = 0 for Si [35] (see Supplemental Material, Fig. S1 [36]), we used a diameter of $D = 840$ nm, which produced the second-order anapole resonance at $\lambda_{\mathrm{res}} = 980$ nm, according to Fig. 2(a). Also shown are the scattering cross section and normalized electromagnetic energy. A peak appears for the energy at minimum scattering cross section. The corresponding normalized
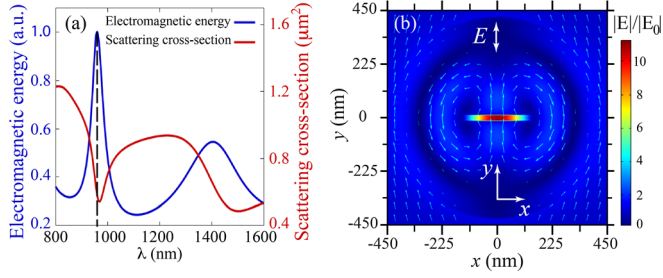
FIG. 2. (a) Scattering cross section and normalized electromagnetic energy as functions of incident wavelength. The vertical dashed line indicates the second-order anapole resonance, featuring maximum electric and magnetic energies inside the nanodisk with minimum scattering values. (b) Normalized electric field profile associated with the second-order anapole mode in (a). The insets in (b) are used to illustrate the direction of oscillation of the electric field component of light.

electromagnetic field profile for this resonant anapole mode is shown in Fig. 2(b), featuring the four field zeros (along the x direction) of the second-order anapole mode. Following calculations analogous to Ref. [38], with eigenmodes of the solid circular nanodisk having Bessel-like profiles, the field profile in Fig. 2(b) comes from the superposition of modes $J_0[(x_{03}/R)r]$ and $J_2[(x_{23}/R)r]$, where x_{ml} indicates the l-order zero of J_m (see Supplemental Material, Fig. S2 [36]). With multipole decomposition analysis we show unambiguously that this second-order mode arises from the interplay between the electric dipole and magnetic quadrupole contributions (see Supplemental Material, Fig. S3 [36]), consistent with reports for large R values [29].

We analyze the optical forces experienced by a 15-nm-radius dielectric nanoparticle ($n_{np} = 2.0$) placed 20 nm above the slotted nanodisk in Fig. 1. Numerical results for the transverse optical forces, i.e., F_x and F_y, are shown in Figs. 3(a) and 3(b), respectively, which were obtained by sweeping the nanoparticle along the xy plane at $z = 120$ nm where Eqs. (3) and (4) were solved. These transverse forces work to localize the nanoparticle at the center of the nanodisk, i.e., at this position the transverse optical force becomes zero. For emphasis, the traces along the $x = 0$ and $y = 0$ planes are shown in Figs. 3(c) and 3(d) for the effective potential in Fig. 1. A minimum potential, i.e., $\mathbf{F}_{xy} = -[(\partial U/\partial x), (\partial U/\partial y)] = \mathbf{0}$, with depth $U < -10\ k_BT$ indicates that the lateral forces will restore the particle to the equilibrium position when Brownian motion or external forces try to move it away from the near-field hot spot.

Along with transverse optical trapping, the nanoparticle experiences a longitudinal force F_z pulling the particle toward the slot as indicated in Fig. 4(a). In the slot region there are higher near-field amplitudes producing stronger forces and stiffer optical trapping. These calculations were also made at $z = 120$ nm along the xy plane. The calculated longitudinal force F_z and transverse effective
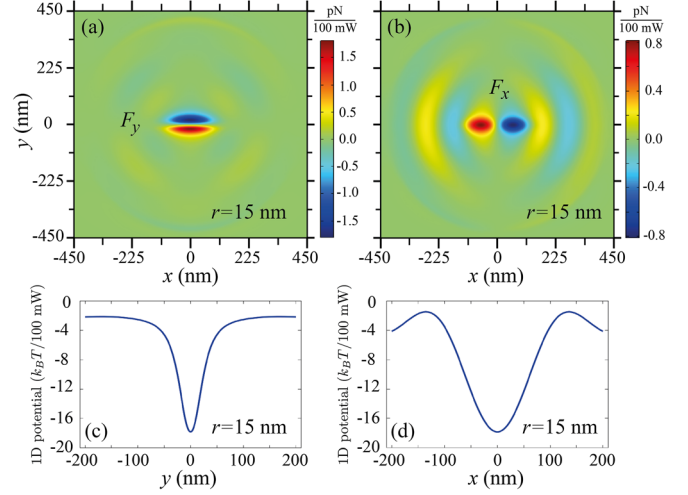

FIG. 3. Transverse optical forces (a) F_x and (b) F_y experienced by a dielectric nanoparticle, with $r = 15$ nm and $n_{np} = 2.0$, placed 20 nm above the nanodisk. (c) and (d) are the traces of the effective potential along the planes (a) $x = 0$ and (b) $y = 0$ for the nanoparticle, respectively.

potential depths as functions of z are shown in Figs. 4(b) and 4(c), respectively, for nanoparticles with $r = 12$ nm, $r = 15$ nm, and $r = 18$ nm. Results were obtained for the center of the nanoparticles from $z = 116$ nm up to $z = 130$ nm. The effective potential depth for these
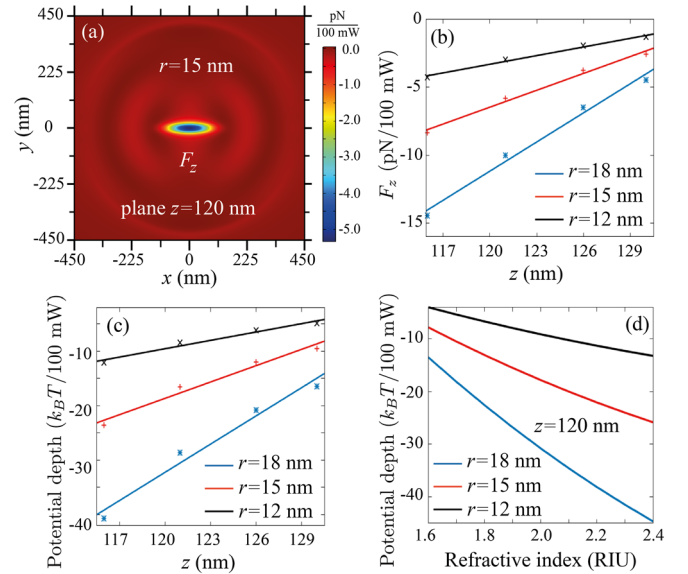

FIG. 4. Longitudinal optical force (F_z) field map generated on a nanoparticle with $r = 15$ nm with the center at $z = 120$ nm. Comparative calculations of (b) longitudinal optical force and (b) the transverse effective potential for nanoparticles with radius $r = 12$ nm, $r = 15$ nm, and $r = 18$ nm, as a function of their center position along the z axis. The results in (a)–(c) were obtained for $n_{np} = 2.0$. (d) Minimum of the effective potential as a function of the nanoparticle refractive index. Calculations for a nanoparticle 20 nm ($z = 120$ nm) away from the top of the nanodisk.

nanoparticles placed at $z = 120$ nm in Fig. 4(d) decreases by decreasing the nanoparticle refractive index. Since the longitudinal trapping force pulls the nanoparticle to the slot region, and stable optical trapping may occur with plasmonic optical potentials around $U \lesssim -6 \, k_B T$ [39], we expect stiff optical trapping of nanoparticles with refractive indexes $n_{np} \geq 1.7$ placed at distances up to 20 nm above the structure (i.e., at $z = 120$ nm). The trapping of nanoparticles with $n_{np} \geq 2.0$ and radius $r \leq 15$ nm should also occur. This proposal is highly competitive with conventional lossy nanoaperture-based plasmonic optical tweezers for studying label-free proteins and their interactions with DNA or small molecules [40]. Significantly, the possibility to use substrates made of silicon-compatible ferromagnetic semiconductors [41] (or externally applied magnetic fields) may allow for enantioselective optical trapping through magneto-optically induced lateral optical forces [42].

Figure 5(a) shows the transverse total optical force pulling a nanoparticle with $n_{np} = 2.0$ and $r = 8$ nm, placed 10 nm above the nanodisk, towards the center of the nanodisk. Since its diameter is smaller than the slot width (25 nm), the nanoparticle can be stably trapped inside the aperture, as shown in Fig. 5(b) with the F_z force field inside the slot. The nanoparticle should then be stably trapped at $z = 45$ nm (almost at the middle height) of the nanodisk inside this region. For convergence purposes, force calculations in Fig. 5(b) were performed using the dipolar approximation, i.e., within the Rayleigh regime [7].

In resonant plasmonic nanostructures heat originates from the Joule effect associated with electronic currents [43]. In contrast to plasmonics, resonant dielectric nanostructures do not have free charge carriers and losses should be negligible. However, we show here the heating of dielectric nanostructures in the presence of high displacement current densities ($\mathbf{J}_d = i\omega\mathbf{D}$, with $\mathbf{D} = \varepsilon\varepsilon_0\mathbf{E}$), especially within the visible and near-infrared regimes where there are relatively high losses [Im(ε)]. Following the rationale of Refs. [43,44], the heat power density for dielectric nanostructures is

$$q(\mathbf{r}) = \frac{1}{2}\text{Re}\{\mathbf{J}_d^*(\mathbf{r}) \cdot \mathbf{E}(\mathbf{r})\} = \frac{\omega}{2}\text{Im}(\varepsilon)\varepsilon_0|\mathbf{E}(\mathbf{r})|^2. \quad (5)$$

The results were obtained at $\lambda = 980$ nm, where Im(ε) = 0 for amorphous silicon, as in Supplemental Material, Fig. S2 [35]. Therefore, the nanostructure does not suffer electromagnetic heating, as verified with numerical calculations (see Fig. 6) using the finite element method (FEM) in COMSOL Multiphysics. Nevertheless, near the visible wavelengths Im(ε) increases with decreasing λ and stronger electromagnetic heating is expected for lower wavelengths. Figure 6(a) shows $q(\mathbf{r})$ for a silicon nanodisk with $R = 390$ nm and $h = 100$ nm, which exhibits the second-order anapole mode at $\lambda = 924$ nm. Since at this resonant wavelength Im(ε) ≈ 0.17 for amorphous silicon (see Supplemental Material, Fig. S2), electromagnetic heating is expected. Indeed, Fig. 6(a) shows that $q(\mathbf{r})$ reaches values above 25×10^{-4} (nW/nm³), i.e., the nanodisk is radiating heat to the surrounding media.

Considering the system initially at room temperature, we calculated the spatial temperature profile by solving the heat diffusion equation under the steady-state condition [44]

$$\nabla \cdot [\kappa(\mathbf{r})\nabla T(\mathbf{r})] = -q(\mathbf{r}), \qquad \text{inside the nanodisk}, \quad (6)$$

$$\nabla \cdot [\kappa(\mathbf{r})\nabla T(\mathbf{r})] = 0, \qquad \text{outside the nanodisk}, \quad (7)$$
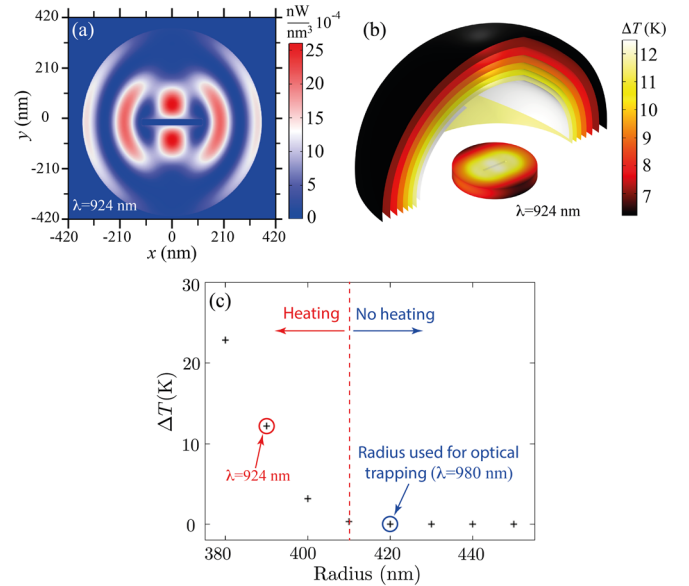
FIG. 6. (a) Numerical results for the electromagnetic heat power density at $\lambda = 924$ nm, at half the height of the nanodisk. (b) Steady-state spatial temperature distribution profile for the system in (a). (c) The maximum temperature increase (due to the excitation of the second-order anapole mode) as function of the nanodisk radius. The regions with and without electromagnetic losses, labeled as heating and no heating, are indicated. The circle within the heating region indicates the radius used for the thermal calculations in (a) and (b), whereas the radius pointed out in the no heating-region corresponds to the radius used for the nanoparticle trapping calculations.
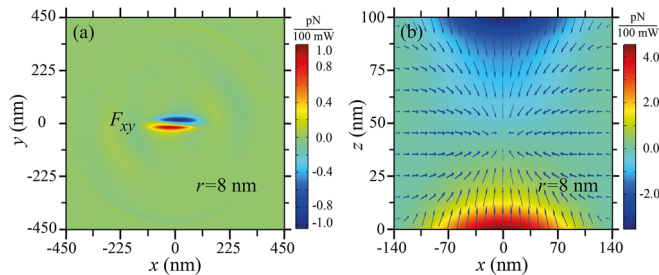

FIG. 5. (a) Transverse total optical force F_{xy} calculated for a nanoparticle with $r = 10$ nm and $n_{np} = 2.0$ with its center at 10 nm away from the nanodisk. (b) Normal optical force (F_z) on the nanoparticle inside the slot region. Numerical results in (b) were obtained within the dipolar approximation.

where $\kappa(\mathbf{r})$ is the thermal conductivity, with $\kappa_{Si} = 1.5$ W/m K for amorphous silicon [45], $\kappa_{water} = 0.61$ W/m K for water (surrounding the nanostructure), and $\kappa_{glass} = 1.38$ W/m K for glass. Numerical results in Fig. 6(b) for the increase in temperature (i.e., $\Delta T = T_f - T_i$) versus T_f indicate the final temperature at each point. The vertical dashed line in Fig. 6(c) illustrates that nanoparticles with radius larger (lower) than $R = 410$ nm produce the second-order anapole modes at wavelengths where negligible (non-negligible) electromagnetic losses occur. Note that for non-negligible electromagnetic losses, convection in the surrounding fluid may constitute a major drawback for stable particle trapping. The radii of the nanodisks used for the calculations in Figs. 6(a) and 6(b) (with $\lambda = 924$ nm) and for the lossless optical trapping ($\lambda = 980$ nm) in Figs. 3–6 are pointed out. These calculations were made using FEM within COMSOL Multiphysics (using the heat-transfer module), under a plane wave illumination with incident power of 1 (mW/μm^2).

In summary, we demonstrated a concept for efficient lossless optical trapping of small nanoparticles, i.e., without heating the structure, which may allow for manipulation of small biological molecules and study their interactions. Instead of plasmonic nanostructures, we use an all-dielectric platform comprising a silicon nanodisk on a glass substrate, surrounded by water. We exploited the second-order anapole mode to create a hot spot at the small slot region, with which nanoparticles with diameters of the order of $D = 20$ nm could be trapped with an incident field wavelength $\lambda = 980$ nm. Nanoparticles smaller than the width of the slot are stably trapped inside the slot, which may find applications in sorting small nanoparticles according to their sizes [46]. On the other hand, larger nanoparticles are stably trapped along the plane perpendicular to the nanodisk axis, as a longitudinal force pushes the nanoparticle towards the region inside the slot and guarantees stiff trapping. The latter result enables further manipulation and processing of the nanoparticle at the aperture surface. This trapping capability for subwavelength particles (small D/λ ratios) is similar to or even higher than most plasmonic counterparts, with the advantage of not heating the structure. The compact design can be extended to 2D arrangements of nanocylinders, enabling practical applications through integration with microfluidic channels.

[*]jrmejia3146@gmail.com

[1] A. Ashkin, Acceleration and Trapping of Particles by Radiation Pressure, Phys. Rev. Lett. **24**, 156 (1970).

[2] A. Ashkin, J. M. Dziedzic, J. E. Bjorkholm, and S. Chu, Observation of a single-beam gradient force optical trap for dielectric particles, Opt. Lett. **11**, 288 (1986).

[3] A. Ashkin and J. Dziedzic, Optical trapping and manipulation of viruses and bacteria, Science **235**, 1517 (1987).

[4] A. Ashkin, J. M. Dziedzic, and T. Yamane, Optical trapping and manipulation of single cells using infrared laser beams, Nature (London) **330**, 769 (1987).

[5] Y. Liu, D. K. Cheng, G. J. Sonek, M. W. Berns, C. F. Chapman, and B. J. Tromberg, Evidence of localized cell heating induced by infrared optical tweezers, Biophys. J. **68**, 2137 (1995).

[6] L. Novotny, R. X. Bian, and X. S. Xie, Theory of Nanometric Optical Tweezers, Phys. Rev. Lett. **79**, 645 (1997).

[7] P. C. Chaumet and M. Nieto-Vesperinas, Time-averaged total force on a dipolar sphere in an electromagnetic field, Opt. Lett. **25**, 1065 (2000).

[8] P. Ben-Abdallah and A. O. E. Moctar, Optical manipulation of neutral nanoparticles suspended in a microfluidic channel, J. Appl. Phys. **99**, 094303 (2006).

[9] A. A. A. Balushi, A. Kotnala, S. Wheaton, R. M. Gelfand, Y. Rajashekara, and R. Gordon, Label-free free-solution nanoaperture optical tweezers for single molecule protein studies, Analyst **140**, 4760 (2015).

[10] D. Gao, W. Ding, M. Nieto-Vesperinas, X. Ding, M. Rahman, T. Zhang, C. T. Lim, and C. W. Qiu, Optical manipulation from the microscale to the nanoscale: Fundamentals, advances and prospects, Light **6**, e17039 (2017).

[11] M. L. Bennink, O. D. Schärer, R. Kanaar, K. Sakata-Sogawa, J. M. Schins, J. S. Kanger, B. G. de Grooth, and J. Greve, Single-molecule manipulation of double-stranded DNA using optical tweezers: Interaction studies of DNA with RecA and YOYO-1, Cytometry **36**, 200 (1999).

[12] P. J. Reece, W. J. Toe, F. Wang, S. Paiman, Q. Gao, H. H. Tan, and C. Jagadish, Characterization of semiconductor nanowires using optical tweezers, Nano Lett. **11**, 2375 (2011).

[13] M. Ploschner, T. Cizmar, M. Mazilu, A. Di Falco, and K. Dholakia, Bidirectional optical sorting of gold nanoparticles, Nano Lett. **12**, 1923 (2012).

[14] Z. Pilát, A. Jonáš, J. Ježek, and P. Zemánek, Effects of infrared optical trapping on *Saccharomyces cerevisiae* in a microfluidic system, Sensors **17**, 2640 (2017).

[15] K. Okamoto and S. Kawata, Radiation Force Exerted on Subwavelength Particles Near a Nanoaperture, Phys. Rev. Lett. **83**, 4534 (1999).

[16] H. Xu and M. Käll, Surface-Plasmon-Enhanced Optical Forces in Silver Nanoaggregates, Phys. Rev. Lett. **89**, 246802 (2002).

[17] M. L. Juan, M. Righini, and R. Quidant, Plasmon nano-optical tweezers, Nat. Photonics **5**, 349 (2011).

[18] A. A. E. Saleh and J. A. Dionne, Toward efficient optical trapping of sub-10-nm particles with coaxial plasmonic apertures, Nano Lett. **12**, 5581 (2012).

[19] D. Yoo, K. L. Gurunatha, H.-K. Choi, D. A. Mohr, C. T. Ertsgaard, R. Gordon, and S.-H. Oh, Low-power trapping of

nanoparticles and proteins with resonant coaxial nanoaperture using 10 nm gap, Nano Lett. **18,** 3637 (2018).

[20] K. Wang and K. B. Crozier, Plasmonic trapping with a gold nanopillar, Chem. Phys. Chem. **13,** 2639 (2012).

[21] D. G. Kotsifaki, V. G. Truong, and S. N. Chormaic, Dynamic multiple nanoparticle trapping using metamaterial plasmonic tweezers, Appl. Phys. Lett. **118,** 021107 (2021).

[22] J. R. Mejía-Salazar and O. N. Oliveira Jr, Plasmonic biosensing: Focus review, Chem. Rev. **118,** 10617 (2018).

[23] A. I. Kuznetsov, A. E. Miroshnichenko, M. L. Brongersma, Y. S. Kivshar, and B. Luk'yanchuk, Optically resonant dielectric nanostructures, Science **354,** aag2472 (2016).

[24] A. E. Miroshnichenko, A. B. Evlyukhin, Y. F. Yu, R. M. Bakker, A. Chipouline, A. I. Kuznetsov, B. Luk'yanchuk, B. N. Chichkov, and Y. S. Kivshar, Nonradiating anapole modes in dielectric nanoparticles, Nat. Commun. **6,** 8069 (2015).

[25] G. Grinblat, Y. Li, M. P. Nielsen, R. F. Oulton, and S. A. Maier, Enhanced third harmonic generation in single germanium nanodisks excited at the anapole mode, Nano Lett. **16,** 4635 (2016).

[26] V. A. Zenin, A. B. Evlyukhin, S. M. Novikov, Y. Yang, R. Malureanu, A. V. Lavrinenko, B. N. Chichkov, and S. I. Bozhevolnyi, Direct amplitude-phase near-field observation of higher-order anapole States, Nano Lett. **17,** 7152 (2017).

[27] B. Luk'yanchuk, R. Paniagua-Domínguez, A. I. Kuznetsov, A. E. Miroshnichenko, and Y. S. Kivshar, Hybrid anapole modes of high-index dielectric nanoparticles, Phys. Rev. A **95,** 063820 (2017).

[28] S.-D. Liu, Z.-X. Wang, W.-J. Wang, J.-D. Chen, and Z.-H. Chen, High Q-factor with the excitation of anapole modes in dielectric split nanodisk arrays, Opt. Express **25,** 22375 (2017).

[29] Y. Yang, V. A. Zenin, and S. I. Bozhevolnyi, Anapole-assisted strong field enhancement in individual all-dielectric nanostructures, ACS Photonics **5,** 1960 (2018).

[30] J. A. Stratton, *Electromagnetic Theory* (McGraw-Hill, New York, 1941).

[31] L. Novotny, Forces in optical near-fields, in *Near-Field Optics and Surface Plasmon Polaritons*, edited by S. Kawata, Collection: Topics in Applied Physics Vol. 81 (Springer, Berlin, Heidelberg, 2001), pp. 123–141, https://doi.org/10.1007/3-540-44552-8_7.

[32] F. A. Sauer, in *Coherent Excitations in Biological Systems*, edited by H. Frohlich and F. Kremer (Springer Berlin Heidelberg, Berlin, Heidelberg, 1983), pp. 134–144.

[33] T. L. McMeekin, M. L. Groves, and N. J. Hipp, Amino acids and serum proteins, in *Advances in Chemistry* (American Chemical Society, Washington, DC, 1964), Vol. 44, Chap. 4, pp. 54–66.

[34] L.-W. Wang and A. Zunger, Pseudopotential calculations of nanoscale CdSe quantum dots, Phys. Rev. B **53,** 9579 (1996).

[35] E. D. Palik, *Handbook of Optical Constants of Solids* (Elsevier Inc., New York, 1985).

[36] See Supplemental Material at http://link.aps.org/supplemental/10.1103/PhysRevLett.127.186803 for a brief description of the wavelength dependence of the imaginary permittivity component, the calculations to demonstrate the symmetry of the second-order anapole mode, and the contributions from multipoles to the scattering cross sections of the slotted nanodisk, which includes Refs. [29,35,37,38].

[37] C. Viviescas and G. Hackenbroich, Quantum theory of multimode fields: Applications to optical resonators, J. Opt. B **6,** 211 (2004).

[38] J. S. T. Gongora, G. Favraud, and A. Fratalocchi, Fundamental and high-order anapoles in all-dielectric metamaterials via Fano-Feshbach modes competition, Nanotechnology **28,** 104001 (2017).

[39] M. Ploschner, M. Mazilu, T. F. Krauss, and K. Dholakia, Optical forces near a nanoantenna, J. Nanophoton. **4,** 041570 (2010).

[40] A. A. Al Balushi and R. Gordon, Label-free free-solution single-molecule protein-small molecule interaction observed by double-nanohole plasmonic trapping, ACS Photonics **1,** 389 (2014).

[41] L. Bi, J. Hu, P. Jiang, H. S. Kim, D. H. Kim, M. C. Onbasli, G. F. Dionne, and C. A. Ross, Magneto-optical thin films for on-chip monolithic integration of non-reciprocal photonic devices, Materials **6,** 5094 (2013).

[42] J. A. Girón-Sedas, J. J. Kingsley-Smith, and F. J. Rodríguez-Fortuño, Lateral optical force on linearly polarized dipoles near a magneto-optical surface based on polarization conversion, Phys. Rev. B **100,** 075419 (2019).

[43] G. Baffou, C. Girard, and R. Quidant, Mapping Heat Origin in Plasmonic Structures, Phys. Rev. Lett. **104,** 136805 (2010).

[44] G. Baffou and R. Quidant, Thermo-plasmonics: Using metallic nanostructures as nano-sources of heat, Laser Photonics Rev. **7,** 171 (2013).

[45] W. Hiroshi and K. Takeshi, Thermal conductivity of amorphous silicon, Jpn. J. Appl. Phys. **35,** 648 (1996).

[46] H. Fujiwara, K. Yamauchitakudo, W. Ishihara, and K. Sasaki, Optical selection and sorting of nanoparticles according to quantum mechanical properties, Sci. Adv. **7,** eabd9551 (2021).